King Saud University

Arabian Journal of Chemistry

www.ksu.edu.sa
www.sciencedirect.com

ORIGINAL ARTICLE

The effect of magnetic nanoparticles containing hyaluronic acid and methotrexate on the expression of genes involved in apoptosis and metastasis in A549 lung cancer cell lines

Jiatai Dou [a], Yanfei Mi [b,*], Sara Daneshmand [c], Mostafa Heidari Majd [d]

[a] *Department of Pharmacy, The 78th Group Army Hospital of Chinese PLA, Mudanjiang 157011, China*
[b] *Respiratory and Critical Care Department, Yulin No2 Hospital, Yulin, Shaanxi 719000, China*
[c] *Department of Pharmaceutics, Faculty of Pharmacy, Zabol University of Medical Sciences, Zabol, Iran*
[d] *Department of Medicinal Chemistry, Faculty of Pharmacy, Zabol University of Medical Sciences, Zabol, Iran*

Abstract Lung cancer has been shown to be resistant to treatment with some chemotherapy drugs due to epithelial-mesenchymal transmission (EMT). Because the rate of cytotoxicity and induction of apoptosis by methotrexate (MTX) is negligible in A549 lung cancer cells, a CD44 positive cell line, we decided to synthesize magnetic nanoparticles (MNPs) containing hyaluronic acid (HA) and MTX to evaluate the effect of CD44 receptor targeting on the expression of genes involved in apoptosis. The TNF genes can modulate the expression of CD44 and implicate carcinogenesis and metastases. Therefore, inhibition of the TNF gene and study of its interaction with the CD44 receptor can determine the success of a treatment method. The results of the MTT assay confirmed that the MNPs-HA-MTX offered better cellular cytotoxic effects on cell viability than free MTX. The real-time PCR test also showed that the Bak1/Bclx ratio was 52.5 times higher than the control. On the other hand, the expression of the TNF gene was severely reduced, which could be due to the binding of HA-moiety of the MNPs-HA-MTX to the receptor and endocytosis. All the results gave us hope that we could increase the effectiveness of methotrexate in lung cancer by targeting the CD44 receptor.

© 2022 The Authors. Published by Elsevier B.V. on behalf of King Saud University. This is an open access article under the CC BY-NC-ND license (http://creativecommons.org/licenses/by-nc-nd/4.0/).

* Corresponding author.
 E-mail address: yanfeimi1979@outlook.com (Y. Mi).
Peer review under responsibility of King Saud University.

Production and hosting by Elsevier

1. Introduction

In most human cancers, multiple genetic mutations occur for a normal cell to turn into a tumor cell. Therefore, the identification and study of genes involved in cancer, especially genes that induce apoptosis can help treat cancer (Hassan et al., 2014; Wong, 2011). For example, the biochemical signs of apoptosis are triggered by the activation of a family of proteases called caspases (Elmore, 2007). Also, it is investigated that the anti-apoptotic Bcl-2 proteins inhibit apoptosis pathways by controlling the activation of caspase proteases. On the other hand, the Bcl-2 family of proteins affects mitochondrial membrane permeability and can control mitochondrial events of apoptosis (Newmeyer et al., 2000; Cory and Adams, 2002). Or, tumor necrosis factor (TNF), a major inflammatory cytokine, plays an important role in the genesis, metastasis, and recurrence of some tumors (Li et al., 2012). Some studies have shown that the presence of TNF in some cancers such as breast, lung, pancreas, and colon, can promote the growth and proliferation of cancer cells which leads to metastasis (Li et al., 2012; Yoshida et al., 2002). Since CD44 receptors are overexpressed on A549 lung cancer cells (Jeannot et al., 2016) and there is a positive correlation between TNF expression and CD44 expression (Mikami et al., 2015), we decided to synthesize magnetic nanoparticles (MNPs) containing hyaluronic acid (HA) and methotrexate (MTX) to investigate its effect on induction of apoptosis in lung cancer cells by assessing the expression of Bak1, Bclx, TNF and Caspase-3 genes.

In recent years, a variety of studies have been performed on HA-based drug carriers to target CD44-mediated cancer cells. HA as a natural polysaccharide has many advantages including enzyme degradation capacity, biocompatibility, non-toxicity, good biodegradability, high hydrophilicity, and the ability to active tumor targeting (Luo et al., 2019; Lee et al., 2020). Because CD44 is overexpressed on many cancer cells, it can be used as a target receptor for active drug delivery to deliver anticancer drugs to the target tumor and also reduce the side effects of chemotherapy drugs on normal cells (Sargazi et al., 2018; Kesharwani et al., 2021). In addition, there are several functional groups, including hydroxyl, carboxyl, and acetamido, in the high molecular weight HA, which both provide good solubility to nanocarriers and can be conjugated to different molecules by covalent bonds (Mero and Campisi, 2014; Sargazi et al., 2018).

MTX is a folic acid antagonist that has anti-cancer effects on breast, gastric, prostate, lung cancers, and certain types of head, neck, and esophagogastric carcinomas (Koźmiński et al., 2020). Because methotrexate has the ability to target folate receptors (FRs), in the past we had synthesized two nanocarriers containing methotrexate and investigated their effect on FRs-negative A549 lung cancer cells (Sargazi et al., 2018; Sargazi et al., 2015). As expected, both nanocarriers did not affect A549 cell lines, so we decided to use the CD44 receptor as a new route for targeted delivery of MTX to lung cancer cells and investigate its effect on induction of apoptosis.

2. Experimental

2.1. Materials

All chemical materials were analytical grade and provided from Merck (Darmstadt, Germany) plus Sigma-Aldrich (St. Louis, MO, USA). Also, methotrexate (MTX), propidium iodide (PI), annexin V-FITC apoptosis detection kit and dialysis bag (MWCO = 7 K_D) were ordered from Sigma-Aldrich. A549 cell lines were ordered from the Pasture Institute cell bank (Tehran, Iran). All necessary cell culture media were purchased from either Gibco (Carlsbad, CA) or Caisson labs (North Logan, UT). A high Pure RNA Isolation Kit and EasyTM cDNA Synthesis kit were acquired from Roche (Rotkreuz, Switzerland) and Pars Tous Biotechnology (Mashhad, Iran), respectively.

2.2. Synthesis of MNPs–HA

The base nanocarrier used in this work has already been synthesized (Heidari Majd et al., 2013). The general structure of these nanoparticles is Fe_3O_4-DPA-PEG-NH_2, which DPA is dopamine and used as a linker between Fe_3O_4 and the polymer. PEG is polyethylene glycol and has an amino end for the joints to other molecules. In the following, we will refer to these nanoparticles as MNPs (Section (A) of Fig. 1).

For binding of HA to MNPs requires the activation of its carboxyl groups. For this purpose, 22 mg (containing 0.055 mmol of carboxyl groups) of HA was poured into a moisture-free 50 ml glass flat bottom flask and mixed with 5 ml of formamide for 2 h by a magnetic stirrer while the temperature of the mixture was controlled at 70 °C using a paraffin bath. After reaching the reaction temperature to room temperature, 22.7 mg (0.11 mmol) of Dicyclohexylcarbodiimide (DCC) and 12.7 mg (0.11 mmol) of N-hydroxysuccinimide (NHS) were added to the mixture, and stirring was then continued for 24 h under argon atmosphere.

Then 176 mg of MNPs (containing 0.055 mmol of NH_2 groups) were dissolved in 5 ml of dimethylformamide and added to the activated-HA in the previous step. After adding 100 μL of triethylamine, the reaction mixture was stirred for 5 h at 60 °C and 18 h at room temperature under argon atmosphere. The final solution (Section (B) of Fig. 1) was poured into Amicon Millipore centrifugal filter with a 10 kDa cut-off and centrifuged at 1700 × g to remove excess material. Finally, the MNPs-HA were separated from the solution by an external magnetic field (Dynamag TM-50 system) and dried by lyophilization. The yield was 47 %.

2.3. Tosylation of hydroxyl groups of HA (MNPs-HA-OTs)

The amount of 50 mg of MNPs-HA that was synthesized in the previous step (containing 0.014 mmol of the hydroxyl group of HA) was completely dispersed in 10 ml of alkaline buffer with pH = 9 at 4 °C for 30 min. Then 3.24 mg (0.017 mmol) of TsCl (p-toluenesulfonyl chloride) was weighed and half of it was added to the reaction mixture and stirred for 1 h at 4 °C. After that, the other half was added and stirring was continued for another 1.5 h. In order to remove unreacted TsCl from the reaction mixture, 10 ml of dichloromethane was added to the reaction mixture and stirred well, then separated from the aqueous solution by a Separatory funnel. Finally, acetone was added to the mixture and the MNPs-HA-OTs was removed by Dynamag TM-50 system and dried by lyophilization. The yield was 61 %.

2.4. Synthesis of MNPs–HA-NH₂

All MNPs-HA-OTs were dispersed in 10 ml of ethylenediamine (EDA) and the reaction was continued for 5 h at 65 °C under argon atmosphere. The precipitate, MNPs–HA-NH_2 (Section (C) of Fig. 1), was washed by acetone and separated by Dynamag TM-50 system. The yield was 65.6 %.
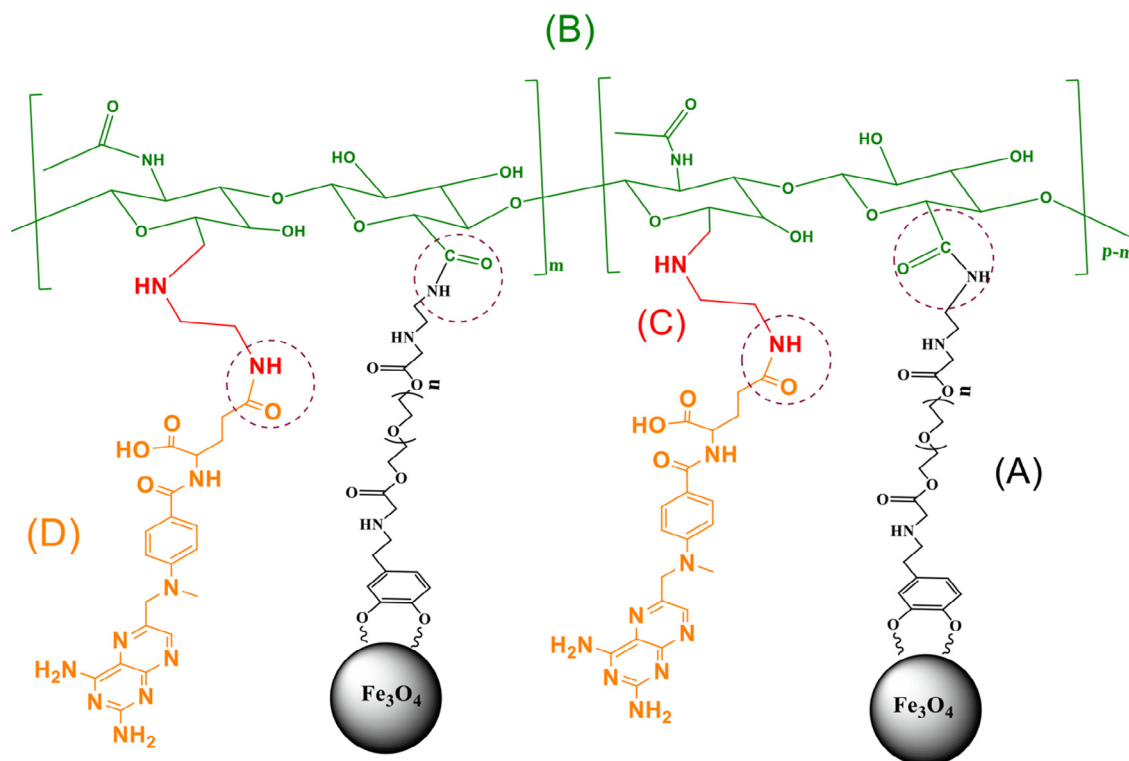
Fig. 1 Schematic representation of the final product, different parts of which are obtained in different steps of synthesis, respectively. (A): MNPs, (B): MNPs-HA, (C): MNPs-HA-NH$_2$ and (D): MNPs-HA-MTX.

2.5. Synthesis of MNPs–HA-MTX

After reading the UV absorption (CECIL, CE1021) of the initial solution of MTX (50 mg in 25 ml DMSO, 0.11 mmol) at 302 nm, 24.97 mg (0.11 mmol) of DCC, 13.92 mg (0.11 mmol) of NHS, and 100 μL of triethylamine were added and stirred overnight at room temperature under argon atmosphere. Unwanted compounds such as dicyclohexylurea were separated by centrifugation at 2300 rpm (10 min, 4 °C). Then all the MNPs–HA-NH$_2$ obtained in the previous step and 20 μL of triethylamine were added to the yellow supernatant (activated-MTX) and stirred for 24 h under argon atmosphere at room temperature. Finally, the MNPs–HA-MTX (Section (D) of Fig. 1) was slowly precipitated by acetone and separated by the Dynamag TM-50 system. The absorption of the final supernatant was checked by a UV spectrophotometer at 302 nm to define the percentage of MTX loading.

2.6. Characterization of MNPs

Infrared Fourier Transform (FTIR) (Shimadzu IR PRES-TIGE 21 spectrophotometer, Tokyo, Japan), FESEM (Mira 3 TESCAN instrument), and particle size analyzer (Malvern Zetasizer_nanoZS, England) methods were used to characterize and identify the synthesized-MNPs in different steps.

2.7. In vitro release test of MTX

To measure the release rate of MTX from MNPs-HA-MTX, two solutions containing 5 mg/mL MNPs were prepared separately in two aqueous media consisting of PBS (pH = 7.4) and sodium acetate buffer (pH = 5.5). The solutions were then sealed in dialysis bags at 37 °C and immersed in own buffer (40 ml) for 72 h. At intervals 0, 24, 48, and 72 h, the percentage of MTX released relative to the initial value was determined using a UV/Vis spectrophotometer at 302 nm where the normal calibration curve for five concentrations of MTX shows the basic equation $y = 0.0469x - 0.1045$ ($R^2 = 0.9974$).

2.8. Cytotoxicity evaluation using MTT assay

In accordance with available guidelines, human lung cancer cell lines A549 were cultured, proliferated, and prepared for MTT testing (Sargazi et al., 2018). After transferring the cells into 96-well culture plates and incubating for 24 h, they were exposed to five different concentrations (from 5 to 500 μM) of MNPs-HA-MTX and free MTX under aseptic conditions for 48 and 72 h. The concentrations of MNPs-HA-MTX and free MTX were equalized together according to the drug loading amount on modified MNPs. Four replicates were considered for each concentration. In addition, four wells were filled with 200 μL of culture medium as a negative control for each period. The MTT test protocol was performed as before works (Shahraki et al., 2019; Sorinezami et al., 2019; Shahraki et al., 2019).

2.9. Real-time PCR for check the apoptosis pathway

To understand the mechanism of induced apoptosis by MNPs-HA-MTX, the PCR method was used to investigate the genes involved in the apoptotic pathways. For this purpose, A549 cells were cultured in two separate flasks. One flask was treated

with 3.8 µM of MNPs-HA-MTX, and the other was selected as a control. After 24 h of incubation, the cells were washed with PBS, detached from the flasks by trypsin and centrifuged at $1000 \times g$ for 5 min, to be ready for isolation of RNA. The isolation of RNA and synthesis of cDNA were performed according to the instructions of the High Pure RNA Isolation Kit and Pars Tous Easy^{TM} cDNA Synthesis Kit, respectively. All details of processes are mentioned in our previous works (Sargazi et al., 2020; Habibi Khorassani et al., 2021; He et al., 2021). To study the apoptotic genes, we used the Real-time PCR assay using Applied Biosystems StepOne^{TM} instrument (Thermo Fisher Scientific, Massachusetts, USA), which detail process, thermal cycling conditions, and calculations were mentioned in our previous work (Ghodsi et al., 2021). The primers used for Real-time PCR analysis were listed in Table 1.

2.10. Agarose gel electrophoresis

Agarose powder (500 mg) was mixed with 50 ml of TBE buffer (consisting of Tris base, Boric acid, EDTA, and distilled water) solution and heated until reach boiling temperature. When the agarose solution cools down to about 50 °C, 2 µL of DNA-safe stain was added to it. Agarose solution was poured into a gel tray and the wells of the gel were made by inserting a comb into the slots in the tray. The new poured gel was placed at 4 °C for 10–15 min until completely solidified. The middle well was assigned to a molecular weight ladder. After adding 2 µL of glycerol and bromophenol blue mixture to samples, left wells were filled with apoptotic genes of untreated cells (Before: TNF, Bclx, and Bak1, respectively) and the wells on the right were filled with apoptotic genes of treated cells (After: Bak1, Bclx, and TNF, respectively). The gel was run at 100 V for 40 min and the cDNA fragments were visualized by UV light of the Gel Doc System (InGenius[3]).

3. Results and discussion

3.1. Characterization of MNPs-HA-MTX

As described in our previous works, the surface of Fe_3O_4 was modified using the dopamine moiety of ''DPA-PEG-NH$_2'$''. Dopamine as an anchoring agent could replace the oleylamine on the surface of Fe_3O_4 NPs (Sargazi et al., 2017; Sargazi and Majd, 2017; Saei et al., 2014). Furthermore, coating layer containing PEG was applied to prevent the agglomeration of

Table 1 Primers used for RT-PCR.

Gene	Primer sequence
Bak1	Forward: TCTGGGACCTCCTTAGCCCT
	Reverse: AATGGGCTCTCACAAGGGTATT
TNF	Forward: CCAGAGGAAGAAGCAACACA
	Reverse: GGAATGAATGCCCACTCCTT
Bclx	Forward: TGGAAAGCGTAGACAAGGAGA
	Reverse: TGCTGCATTGTTCCCATAGA
Caspase-3	Forward: TGCAGTCATTATGAGAGGCAAT
	Reverse: AAGGTTTGAGCCTTTGACCA
GAPDH	Forward: TTGCCATCAATGACCCCTTCA
	Reverse: CGCCCCACTTGATTTTGGA

MNPs, and to conjugate targeting moieties via covalent bonding. The final size of the MNPs (Section (A) of Fig. 1) was 13 nm using FESEM (Saei et al., 2014).

Two common receptors for active targeting of cancer cells are CD44 and FR, which can increase receptor-mediated endocytosis of chemotherapy drugs (Zhang et al., 2022; Yan et al., 2019). In addition, the presence of hydrophilic ligands on the surface of MNPs can increase the systemic distribution and also reduce the side effects of anticancer drugs by active targeting. Because in an aqueous solution such as blood, hydrophobic MNPs tend to aggregate, and therefore, the attachment of a hydrophilic group on their surface can provide sufficient aqueous thermodynamic stability (Singh et al., 2014). For this reason, hyaluronic acid (HA) and methotrexate (MTX), which have a high affinity for the receptors, were conjugated to MNPs. Conjugation of the targeting agents was performed by the formation of amide bonds between the free amine groups ($-NH_2$) of MNPs and the activated carboxyl groups of MTX and HA (dotted line circles in Fig. 1).

FTIR is a spectroscopic method that can measure the vibration and rotation of molecules under the influence of infrared radiation and record changes in various steps of synthesis (Faghihzadeh et al., 2016). As shown in Fig. 2, absorptions at 3402 and 3433 cm^{-1} related to the primary aliphatic amines (Fig. 2A) have been replaced by strong absorption at 3458 cm^{-1} related to the hydroxyl groups of HA (Fig. 2B). In addition, absorption at 1727 cm^{-1} well confirms the presence of carboxylic groups of HA on the surface of the MNPs (Fig. 2B). After the addition of EDA to the HA moiety of MNPs (Section (C) of Fig. 1), an absorption peak appeared in 1597 cm^{-1}, which is attributed to the N$-$H bending of the primary amine groups. Besides that, two absorption peaks at 3402 and 3433 cm^{-1} and also the absorption peak at 1327 cm^{-1} (C$-$N stretching) confirmed the free amine groups located at the end of modified-MNPs (Fig. 2C). Finally, after conjugation of MTX to MNPs-HA-NH$_2$ (Section (D) of Fig. 1), the absorption of the amide and carboxylic acid groups appeared in 1616 and 1689 cm^{-1}, respectively (Fig. 2D).

Nanotechnology has been shown to fill gaps in the biological and physical sciences, especially in medicine and nano-based drug delivery systems. MNPs composed of magnetite (Fe_3O_4) which possess superparamagnetic properties and proper size can employ as biosensors, contrast agents in magnetic resonance imaging (MRI), drug delivery vehicles, and thermal seeds in magnetic hyperthermia therapy (MHT) (Patra et al., 2018; Mitchell et al., 2021). It has been proven that in order to take advantage of the unique properties of MNPs, the size, shape, and surface chemistry of them must be optimized to achieve the best cell adsorption, bio-distribution, and blood circulation half-life (Hoshyar et al., 2016). Therefore, we conjugate the HA and MTX on the surface of MNPs, to help target drug delivery, and improve the bio-availability and therapeutic index of anticancer drugs.

Tumor blood vessels can be diagnosed with abnormalities such as a high proliferation rate of endothelial cells, abnormal shapes of pericytes, and high vascular permeability (Azzi et al., 2013). The enhanced permeability and retention (EPR)-based drug delivery depends on various factors such as the size, shape, and morphology of the MNPs. Several studies confirmed that tumor vessels permit the passage of MNPs ranging from 40 to 200 nm. On the other hand, rigid particles with average size below 200 nm have the highest tendency for long
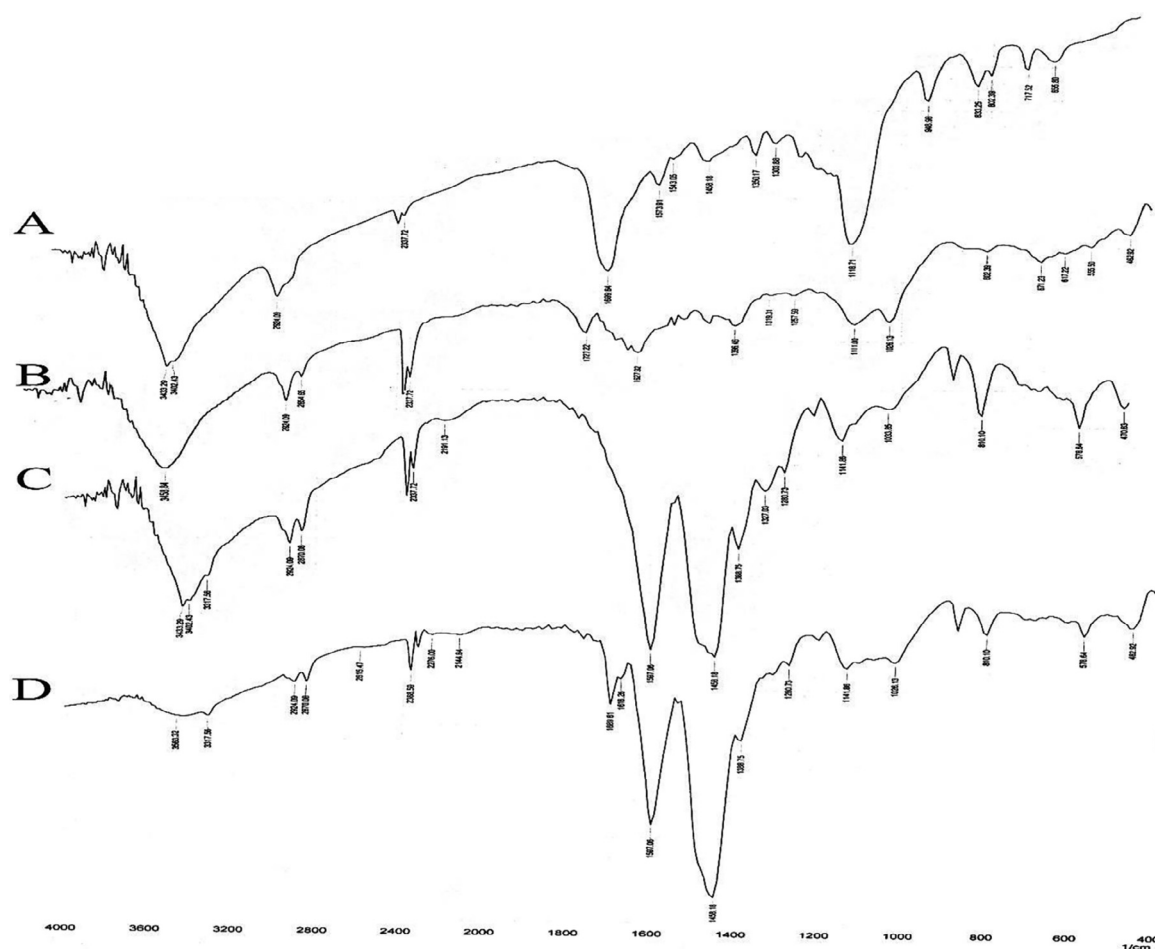
Fig. 2 FTIR spectra of (A): MNPs, (B): MNPs-HA, (C): MNPs-HA-NH2 and (D): MNPs-HA-MTX.

circulation, to avoid renal filtration and clearance of them by the reticuloendothelial system (RES) (Subhan et al., 2021). Therefore, we used the FESEM method to know the morphology and size of MNPs after conjugation of the targeting agents. As seen in Fig. 3A, the average size of the MNPs-HA-MTX was increased after anchoring modifier groups to about 103 nm.

Since the main base of the synthesized MNPs is HA as a hydrophilic polysaccharide (see Fig. 1), when particles were prepared for FESEM imaging, may stick together due to the formation of hydrogen bonds (Payne et al., 2018). Also, if pay attention to the morphology of MNPs in Fig. 3A, can see structural similarities, including their linear and tube-like shape, which is close to the schematic structure in Fig. 1.

Since MNPs in aqueous suspensions are stabilized by electrostatic repulsion of electrical charges on their surface, it is necessary to measure their surface charge and size in diluted aqueous solution (Nguyen et al., 2014). The dispersion quality was usually measured by Dynamic Light Scattering (DLS) and zeta potential methods. Fig. 3B shows that the size calculated by DLS is 73.04 nm and is slightly less than the size obtained by FESEM, which may be due to the presence of water around the MNPs-HA-MTX and the reduction of hydrogen bonding between HA molecules (Gudkov et al., 2020; Tilaki et al., 2007; Stepan et al., 2022). Also, it has been proven that the size

of MNPs in suspensions is affected by electrical charges and absorbed surface layers and may change as the suspension dilutes (Kurlyandskaya et al., 2017).

Highly dispersed particles have zeta potential values greater than $+30$ mV or less than -30 mV to present sufficient repulsive force and useful colloidal stability. The zeta potential of MNPs-HA-MTX was -40.9 mV (Fig. 3C) and proved that the carboxyl groups relating to HA and FA could play a key role in surface charge density and stabilizing in aqueous solutions.

3.2. Loading capacity and sustained release of MNPs-HA-MTX

Typically, the conjugation between the carriers and the drug molecules is either through a weak electrostatic bond or through a covalent bond. These systems are distributed as pro-drugs in the blood circulation system and can reach the target organ, tissue, or cell, and then the drug is activated by cleavage of the bond between them. Covalent bond formation increases drug loading capacity, prolongs drug circulation in the blood, and controls drug release in the target organ (Theodosis-Nobelos et al., 2020). In this work, the amide bonds are the main linker between the different parts of the modified MNPs (dotted line circles in Fig. 1). It has been
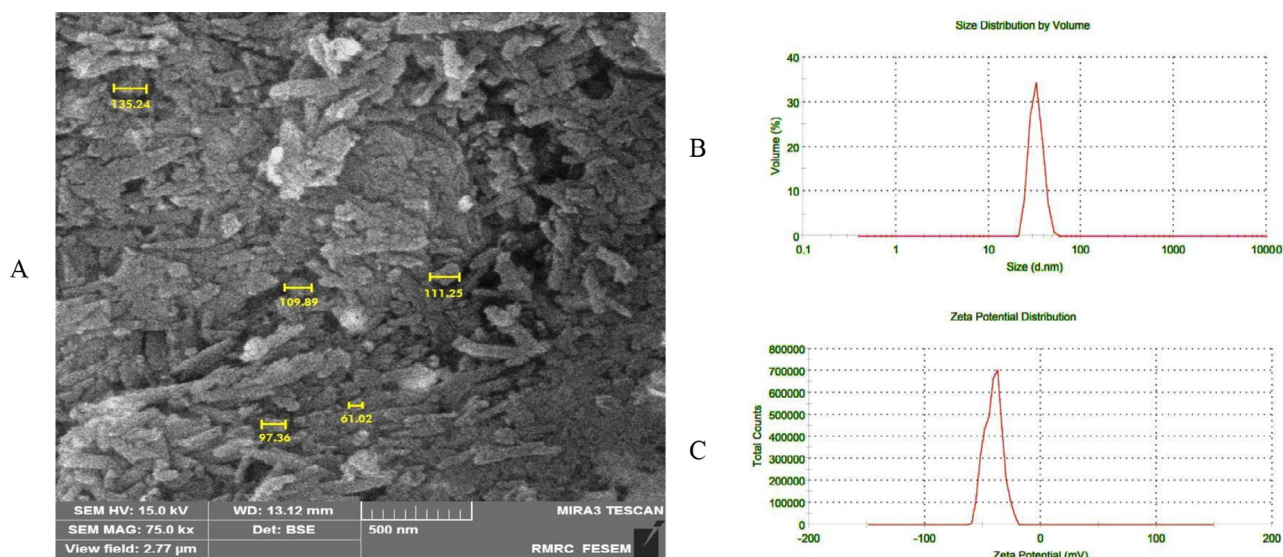
Fig. 3 A) Shows the FESEM image of the MNPs-HA-MTX. The magnification used for this imaging was 75 kx. B and C) show the size distribution and zeta potential of MNPs-HA-MTX in water solution. Zeta potential is usually measured from $+100$ mV to -100 mV.

established that amide linkers were broken in response to acidic signals within the tumor, leading to drug detachment from the carrier (He et al., 2020).

On the other hand, drug-loading content and drug-loading efficiency are two significant indexes, especially when a hydrophobic drug with known side effects is loaded on the MNPs (Shen et al., 2017). The drug-loading content, which reflects the mass ratio of the drugs to the synthesized MNPs, was calculated to be 42.94 % and was obtained from the following formula:

$$Drug\ loading\ content\%$$
$$= \frac{Mass\ of\ the\ loaded\ drug}{Initial\ mass\ of\ MNPs\ before\ loading} \times 100 \qquad (1)$$

And drug-loading efficiency, which reflects the ratio of loaded drugs to the total amount of drugs used, was calculated to be 88.11 % and was obtained from the following formula:

$$Drug\ loading\ efficiency\%$$
$$= \frac{Mass\ of\ the\ loaded\ drug}{Initial\ mass\ of\ drugs\ before\ loading} \times 100 \qquad (2)$$

In most cases, achieving high drug-loading content is more difficult than achieving high drug-loading efficiency. Usually, the drug loading content is related to the structure and physical and chemical properties of the nanocarrier. The larger surface area or larger pore volume of the nanocarrier provides better drug loading content (Yu et al., 2017). While, drug loading efficiency is defined by drug loading mechanism, drug mass, and other experimental conditions of drug loading (Zhang et al., 2016). When, the drug-loading mechanism is physically and electrostatically, the drug-loading efficiency decreases, while the drug-loading process through coordinate and covalent bonds often leads to high drug-loading efficiency (Cao et al., 2019).

In addition, the presence of covalent bonds leads to sustainable drug release, because it needs a suitable environment to cleavage the bond. Many studies have confirmed that modified-MNPs enter the lysosome by receptor-mediated

endocytosis and undergo hydrolysis (Zhang et al., 2010). On the other hand, many areas inside tumors, especially the lysosome, are hypoxic and acidic (Pranantyo et al., 2021); so we investigated drug release from MNPs in two environments with different pHs. Table 2 shows the MTX release rate from MNPs-HA-MTX in two different environments (pH = 5.5 and 7.4). Because amide bonds could undergo hydrolysis in cancer cells' acidic lysosomes (Ren et al., 2014), the release rate of MTX was higher at pH 5.5 and was able to show a sustainable drug release system.

3.3. In vitro cytotoxicity assessment

To evaluate the cytotoxicity of MNPs-HA-MTX, the A549 human lung adenocarcinoma cell line was selected, which according to previous research has low levels of FRs, while expressing high levels of CD44 receptors (Jeannot et al., 2016; Álvarez-González et al., 2020). On the one hand, MTX has the ability to target FRs, and in our previous works (Sargazi et al., 2018; Sargazi et al., 2015), its effect on FR-positive cell lines has been demonstrated. On the other hand, previous research has shown that the effect of MTX on the A549 cell line is negligible (Morandi et al., 2017). Therefore, the A549 cell line was selected to investigate the role of HA in CD44 receptor targeting as well as the effect of MNPs-HA-MTX on lung cancer through receptor-mediated endocytosis by HA.

As can be concluded from the IC_{50} results of the MTT assay (Table 3), the MNPs-HA-MTX offered better cellular cytotoxic effects on cell viability than free MTX. The viability of A549 cell lines at both 48 and 72 h of culture is dependent on the time and concentration of MNPs-HA-MTX (Fig. 4), which reaffirms that the presence of HA in the structure of MNPs significantly increases the effect of MTX on the A549 cell line. Our previous work (Sargazi et al., 2015) confirmed that free MTX at concentrations below 16 μM did no effect on the A549 lung cancer cell line. Therefore, we decided to increase the drug concentration range in the present work.

Table 2 Shows the percentage of MTX release at different times and at two different pHs. The UV absorption of the released MTX is read at 302 nm by a UV spectrophotometer. Due to the acidic environment at pH 5.5, amide bond breakage occurs more easily.

	0 h	24 h	48 h	72 h
pH = 7.4	0	1.13 %	3.58 %	4.81 %
pH = 5.5	0	8.41 %	29.24 %	53.86 %

Table 3 The IC$_{50}$ (μM) values obtained from MTT test.

Compounds	48 h	72 h
Free MTX	–	198
MNPs-HA-MTX	161	10.1

As can be seen in Fig. 4, free MTX at only 500 μM was able to decrease cell viability to 37 % relative to control. Therefore, we can well guess the role of the CD44 receptor in MTX endocytosis into the lung cancer cell line and hope that a nano-drug containing HA can increase the efficacy of methotrexate.

3.4. The apoptosis pathway of MNPs-HA-MTX

There are numerous reports that epithelial-mesenchymal transmission (EMT) is involved in resistance to chemotherapy drugs in several kinds of cancers, including lung cancer (Ojima et al., 2021). Also, it has been revealed that MTX can induce EMT in the human A549 cancer cell line which may affect apoptosis, a known method for programmed cell death (Yu et al., 2021). Since there was not enough information to induce apoptosis by MTX on the A549 cell line and also cytotoxic effects of MTX on the cell line were negligible, we decided to investigate the expression of genes involved in apoptosis induced by MNPs-HA-MTX. On the other hand, we speculate that the conjugation of targeting agents like HA on MNPs and receptor-mediated endocytosis of chemotherapy drugs may affect the expression of apoptotic genes. Because in our previous works, the presence of folic acid in the structure of complexes activated the mitochondrial pathway of apoptosis and increased Bak1 gene expression (Yang et al., 2021; Liu et al., 2019). The Bcl-2 family of proteins (Bak1 and Bclx) is the major regulators of apoptosis, and examination of their expression reveals detailed knowledge of the mitochondrial-mediated apoptosis pathway. As the results in Table 4 shown, the expression of the pro-apoptotic gene (Bak1) of this family was 1949.6 which lead to the Bak1/Bclx ratio equal to 52.5.

Also, the possible association of Bak1/Bclx ratios with the apoptotic coordinating enzyme, caspase-3, could confirm the Bak-sensitive (intrinsic) mitochondrial pathway. The results of Table 4 confirm that the expression of the caspase-3 gene in MNPs-HA-MTX treated cells increased 28-fold against control.

TNF responds differently in various cell types, in some cells causes apoptosis and necrosis, and in others induce cell proliferation. For example, TNF especially TNF-alpha modulates the expression of CD44 and is implicated in carcinogenesis and metastases. Therefore, inhibition of the TNF gene and study of its interaction with the CD44 receptor can determine the success of a treatment method. Results of the Real-time-PCR test showed that the expression of the TNF gene was severely reduced (Fig. 5A), which could be due to the binding of HA-moiety of the MNPs-HA-MTX to the receptor and endocytosis. In a similar study, Liu et al. synthesized chondroitin sulfate (CS) -modified PLGA NPs for targeted delivery of 10-hydroxycampotoxin. CS has a structure similar to HA and can therefore bind to the CD44 receptor. The results showed that HCPT/CS-CN-PLGA NP significantly reduced TNF-α levels in the colon cancer cell line (Tzifi et al., 2012).
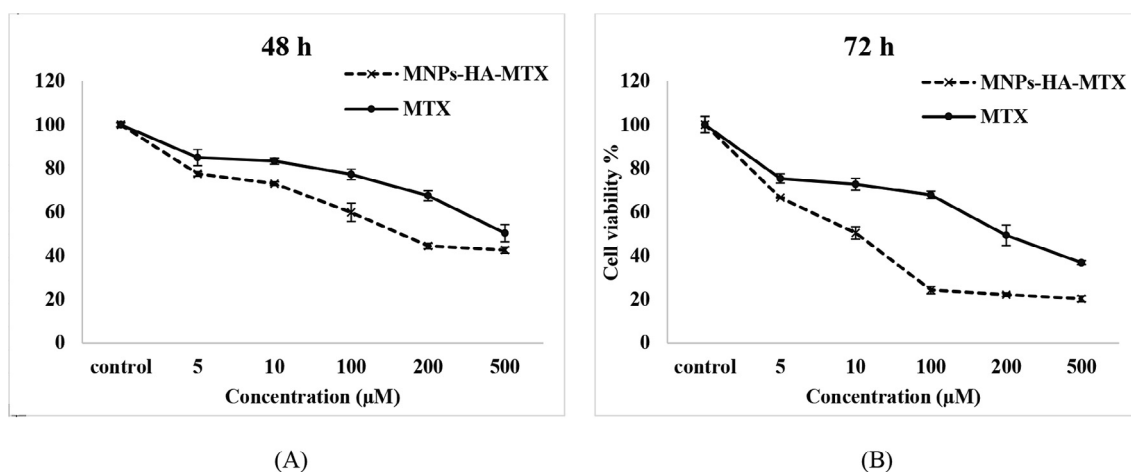

Fig. 4 Cytotoxicity evaluation of MNPs-HA-MTX and free MTX on A549 cell lines after 48 and 72 h of exposure. Free MTX was able to affect lung cancer cell line only at high concentrations and after 72 h.

Table 4 Evaluation of genes expression involved in apoptosis by real-time PCR (Applied Biosystems StepOne™ instrument; Thermo Fisher Scientific, Massachusetts, USA). RQ is equal with $2^{(-\Delta\Delta CT)}$. †GAPDH is endogenous control.

Genes	Sample	CT (mean)	ΔCT	ΔΔCT	RQ
Bclx	Control	21.803	5.028	0	1
	MNPs-HA-MTX	19.97	−0.186	−5.214	37.12
BAK1	Control	25.704	8.929	0	1
	MNPs-HA-MTX	18.16	−1.996	−10.929	1949.6
TNF	Control	25.841	9.066	0	1
	MNPs-HA-MTX	36.32	16.164	7.098	0.0073
Caspase-3	Control	30.107	13.332	0	1
	MNPs-HA-MTX	28.68	8.524	−4.808	28.01
GAPDH †	Control	16.775			
	MNPs-HA-MTX	20.156			

(A)   (B)
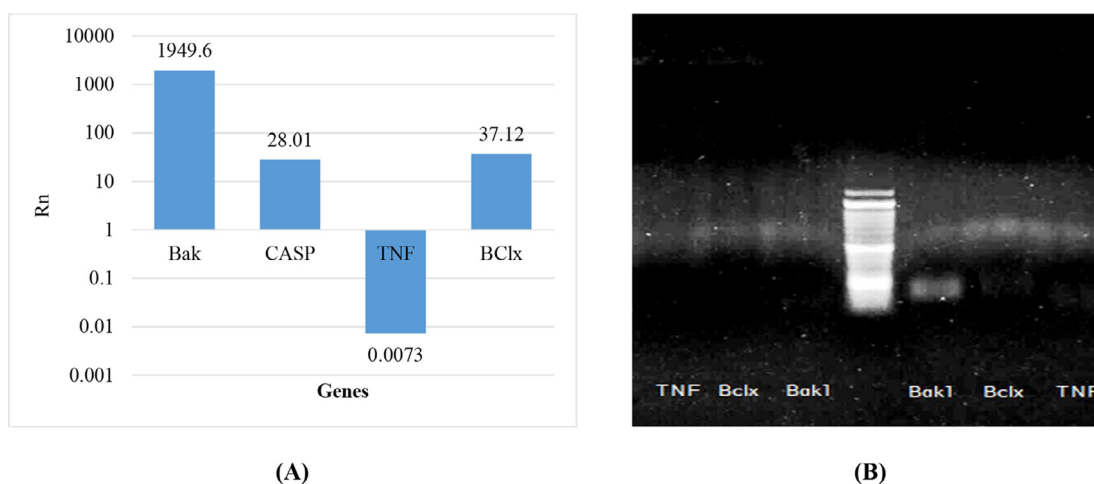
Fig. 5 (A) Logarithmic diagram related to the expression of genes involved in apoptosis. The baseline is 1 and gene expression is measured against control. (B) Agarose gel electrophoresis shows the expression of Bclx, Bak1, and TNF genes in A549 cell lines. Real-time PCR amplified products on the agarose gel.

3.5. DNA fragmentation assay of apoptosis genes using gel electrophoresis

The Bcl-2 protein family that is associated with apoptosis includes two groups: one is the genes that inhibit apoptosis (Bcl-Xl, Bcl-2, Bclx, Mcl-1, etc.) and the other is the genes that induce apoptosis (Bak1, Bad, Bax, Bicycles, etc.) (Brooks et al., 2007). Therefore, increased expression of pro-apoptotic gene Bak1 and Bak1/Bclx ratio indicates induction of apoptosis in the A549 lung cell line. On the other hand, TNF protein is highly expressed in the cancer microenvironment and modulates CD44 expression in various types of cancer (Li et al., 2012). Therefore, the use of CD44 receptor targeting compounds can affect the expression of the TNF gene and prevent cancer metastasis. Agarose gel electrophoresis of PCR products of TNF, Bak1, and Bclx genes treated with MNPs-HA-MTX showed that only the expression of Bak1 protein was increased and the expression of the other two genes (TNF and Bclx) has not increased compared to it (Fig. 5B). Thus, increased Bak1 expression provides the necessary gateway for mitochondrial damage, followed by the permeability of the mitochondrial outer membrane leading to the release of apoptogenic agents in the cell (Brooks et al., 2007).

4. Conclusions

Due to the fact that methotrexate could not have beneficial therapeutic effects on the A549 lung cancer cell line and may develop epithelial-mesenchymal transmission-dependent drug resistance, MNPs-HA-MTX was synthesized. The results of the MTT assay confirmed that MNPs-HA-MTX shows a better time- and dose-dependent cytotoxic effect on the A549 cancer cell line than free MTX. The apoptotic pathway was identified using real-time PCR and confirmed that MNPs-HA-MTX could activate the mitochondrial pathway of apoptosis and increase Bak1 protein levels. On the other hand, the use of CD44 receptor targeting compounds can reduce TNF expression and may prevent cancer metastasis. All the results cleared that targeting the CD44 receptor and endocytosis could increase the effectiveness of MTX in lung cancer.

Declaration of Competing Interest

The authors declare that they have no known competing financial interests or personal relationships that could have appeared to influence the work reported in this paper.

References

Álvarez-González, B., Rozalen, M., Fernández-Perales, M., et al, 2020. Methotrexate Gold Nanocarriers: Loading and Release Study: Its Activity in Colon and Lung. Cancer Cells 25, 6049.

Azzi, S., Hebda, J.K., Gavard, J., 2013. Vascular permeability and drug delivery in cancers. Front Oncol 3, 211. https://doi.org/10.3389/fonc.2013.00211.

Brooks, C., Wei, Q., Feng, L., et al, 2007. Bak regulates mitochondrial morphology and pathology during apoptosis by interacting with mitofusins. Proc. National Acad. Sci. 104, 11649–11654. https://doi.org/10.1073/pnas.0703976104.

Cao, Z., Li, W., Liu, R., et al, 2019. pH- and enzyme-triggered drug release as an important process in the design of anti-tumor drug delivery systems. Biomed. Pharmacother. 118,. https://doi.org/10.1016/j.biopha.2019.109340 109340.

Cory, S., Adams, J.M., 2002. The Bcl2 family: regulators of the cellular life-or-death switch. Nat. Rev. Cancer 2, 647–656. https://doi.org/10.1038/nrc883.

Elmore, S., 2007. Apoptosis: a review of programmed cell death. Toxicol Pathol 35, 495–516. https://doi.org/10.1080/01926230701320337.

Faghihzadeh, F., Anaya, N.M., Schifman, L.A., Oyanedel-Craver, V., 2016. Fourier transform infrared spectroscopy to assess molecular-level changes in microorganisms exposed to nanoparticles. Nanotechnol. Environ. Eng. 1, 1. https://doi.org/10.1007/s41204-016-0001-8.

Ghodsi, F., Shahraki, M., Habibi-Khorassani, S.M., et al, 2021. Kinetic Modeling on Mitoxantrone Release from Hyaluronic MNP as a Drug Delivery System Chemical Methodologies. Chem. Methodol. 5, 30–34. https://doi.org/10.22034/chemm.2021.118506.

Gudkov, S.V., Baimler, I.V., Uvarov, O.V., et al, 2020. Influence of the concentration of Fe and Cu nanoparticles on the dynamics of the size distribution of nanoparticles. Front. Phys. 8, 578. https://doi.org/10.3389/fphy.2020.622551.

Habibi Khorassani, S.M., Ghodsi, F., Arezomandan, H., et al, 2021. In Vitro Apoptosis Evaluation and Kinetic Modeling onto Cyclodextrin-Based Host-Guest Magnetic Nanoparticles Containing Methotrexate and Tamoxifen. BioNanoScience. https://doi.org/10.1007/s12668-021-00877-8.

Hassan, M., Watari, H., AbuAlmaaty, A., et al, 2014. Apoptosis and molecular targeting therapy in cancer. Biomed Res. Int. 2014, 150845. https://doi.org/10.1155/2014/150845.

He, Q., Chen, J., Yan, J., et al, 2020. Tumor microenvironment responsive drug delivery systems. Asian J. Pharm. Sci. 15, 416–448. https://doi.org/10.1016/j.ajps.2019.08.003.

He, C., Heidari Majd, M., Shiri, F., Shahraki, S., 2021. Palladium and platinum complexes of folic acid as new drug delivery systems for treatment of breast cancer cells. J. Mol. Struct. 1229. https://doi.org/10.1016/j.molstruc.2020.129806.

Heidari Majd, M., Asgari, D., Barar, J., et al, 2013. Tamoxifen loaded folic acid armed PEGylated magnetic nanoparticles for targeted imaging and therapy of cancer. Colloids Surf., B 106, 117–125. https://doi.org/10.1016/j.colsurfb.2013.01.051.

Hoshyar, N., Gray, S., Han, H., Bao, G., 2016. The effect of nanoparticle size on in vivo pharmacokinetics and cellular interaction. Nanomedicine 11, 673–692. https://doi.org/10.2217/nnm.16.5.

Jeannot, V., Mazzaferro, S., Lavaud, J., et al, 2016. Targeting CD44 receptor-positive lung tumors using polysaccharide-based nanocarriers: Influence of nanoparticle size and administration route. Nanomed. Nanotechnol. Biol. Med. 12, 921–932. https://doi.org/10.1016/j.nano.2015.11.018.

Kesharwani, P., Chadar, R., Sheikh, A., et al, 2021. CD44-Targeted Nanocarrier for Cancer Therapy. Front. Pharmacol. 12,. https://doi.org/10.3389/fphar.2021.800481 800481.

Koźmiński, P., Halik, P.K., Chesori, R., Gniazdowska, E., 2020. Overview of Dual-Acting Drug Methotrexate in Different Neuro-

logical Diseases, Autoimmune Pathologies and Cancers. Int. J. Mol. Sci. 21, 3483. https://doi.org/10.3390/ijms21103483.

Kurlyandskaya, G.V., Litvinova, L.S., Safronov, A.P., et al, 2017. Water-based suspensions of iron oxide nanoparticles with electrostatic or steric stabilization by chitosan: fabrication, characterization and biocompatibility. Sensors (Basel) 17, 2605. https://doi.org/10.3390/s17112605.

Lee, S.Y., Kang, M.S., Jeong, W.Y., et al, 2020. Hyaluronic Acid-Based Theranostic Nanomedicines for Targeted Cancer Therapy. Cancers 12, 940. https://doi.org/10.3390/cancers12040940.

Li, J., Zha, X.M., Wang, R., et al, 2012. Regulation of CD44 expression by tumor necrosis factor-α and its potential role in breast cancer cell migration. Biomed. Pharmacotherapy = Biomed. Pharmacotherapie 66, 144–150. https://doi.org/10.1016/j.biopha.2011.11.021.

Liu, Z.-L., Li, L.-F., Xia, S.-S., et al, 2019. Chondroitin sulfate modification enhances the targeting and therapeutic effect of nanomedicine on AOM/DSS-induced mouse colon cancer. J. Drug Delivery Sci. Technol. 52, 1–7. https://doi.org/10.1016/j.jddst.2019.04.010.

Luo, Z., Dai, Y., Gao, H., 2019. Development and application of hyaluronic acid in tumor targeting drug delivery. Acta Pharm. Sin. B 9, 1099–1112. https://doi.org/10.1016/j.apsb.2019.06.004.

Mero, A., Campisi, M., 2014. Hyaluronic Acid Bioconjugates for the Delivery of Bioactive. Molecules 6, 346–369.

Mikami, S., Mizuno, R., Kosaka, T., et al, 2015. Expression of TNF-α and CD44 is implicated in poor prognosis, cancer cell invasion, metastasis and resistance to the sunitinib treatment in clear cell renal cell carcinomas. Int. J. Cancer 136, 1504–1514. https://doi.org/10.1002/ijc.29137.

Mitchell, M.J., Billingsley, M.M., Haley, R.M., et al, 2021. Engineering precision nanoparticles for drug delivery. Nat. Rev. Drug Discovery 20, 101–124. https://doi.org/10.1038/s41573-020-0090-8.

Morandi, A., Taddei, M.L., Chiarugi, P., Giannoni, E., 2017. Targeting the Metabolic Reprogramming That Controls Epithelial-to-Mesenchymal Transition in Aggressive Tumors. Front. Oncol. 7. https://doi.org/10.3389/fonc.2017.00040.

Newmeyer, D.D., Bossy-Wetzel, E., Kluck, R.M., et al, 2000. Bcl-xL does not inhibit the function of Apaf-1. Cell Death Differ. 7, 402–407. https://doi.org/10.1038/sj.cdd.4400665.

Nguyen, V.S., Rouxel, D., Vincent, B., 2014. Dispersion of nanoparticles: From organic solvents to polymer solutions. Ultrason. Sonochem. 21, 149–153. https://doi.org/10.1016/j.ultsonch.2013.07.015.

Ojima, T., Kawami, M., Yumoto, R., Takano, M., 2021. Differential mechanisms underlying methotrexate-induced cell death and epithelial-mesenchymal transition in A549 cells. Toxicol. Res. 37, 293–300. https://doi.org/10.1007/s43188-020-00067-w.

Patra, J.K., Das, G., Fraceto, L.F., et al, 2018. Nano based drug delivery systems: recent developments and future prospects. J. Nanobiotechnol. 16, 71. https://doi.org/10.1186/s12951-018-0392-8.

Payne, W.M., Svechkarev, D., Kyrychenko, A., Mohs, A.M., 2018. The role of hydrophobic modification on hyaluronic acid dynamics and self-assembly. Carbohydr. Polym. 182, 132–141. https://doi.org/10.1016/j.carbpol.2017.10.054.

Pranantyo, D., Kang, E.-T., Chan-Park, M.B., 2021. Smart nanomicelles with bacterial infection-responsive disassembly for selective antimicrobial applications. Biomater. Sci. 9, 1627–1638. https://doi.org/10.1039/D0BM01382J.

Ren, D., Kratz, F., Wang, S.-W., 2014. Engineered drug-protein nanoparticle complexes for folate receptor targeting. Biochem. Eng. J. 89, 33–41. https://doi.org/10.1016/j.bej.2013.09.008.

Saei, A.A., Barzegari, A., Majd, M.H., et al, 2014. Fe3O4 nanoparticles engineered for plasmid DNA delivery to Escherichia coli. J. Nanopart. Res. 16. https://doi.org/10.1007/s11051-014-2521-0.

Sargazi, A., Kuhestani, K., Nahoki, T.N., Majd, M.H., 2015. Specific targeting of folate receptor by methotrexate conjugated modified

magnetic nanoparticles: Enzymatic release and cytotoxic study. Int. J. Pharmaceut. Sci. Res. 6, 5047.

Sargazi, A., Aliabadi, A., Rahdari, A., et al, 2017. A simple and fast method for magnetic solid phase extraction of ochratoxin A. J. Braz. Chem. Soc. 28, 950–959. https://doi.org/10.21577/0103-5053.20160245.

Sargazi, A., Kamali, N., Shiri, F., Heidari Majd, M., 2018. Hyaluronic acid/polyethylene glycol nanoparticles for controlled delivery of mitoxantrone. Artif. Cells Nanomed. Biotechnol. 46, 500–509. https://doi.org/10.1080/21691401.2017.1324462.

Sargazi, A., Shiri, F., Keikha, S., Majd, M.H., 2018. Hyaluronan magnetic nanoparticle for mitoxantrone delivery toward CD44-positive cancer cells. Colloids Surf., B 171, 150–158. https://doi.org/10.1016/j.colsurfb.2018.07.025.

Sargazi, A., Barani, A., Heidari Majd, M., 2020. Synthesis and Apoptotic Efficacy of Biosynthesized Silver Nanoparticles Using Acacia luciana Flower Extract in MCF-7 Breast Cancer Cells: Activation of Bak1 and Bclx for Cancer Therapy. BioNanoScience 10, 683–689. https://doi.org/10.1007/s12668-020-00753-x.

Sargazi, A., Majd, M.H., 2017. Different applications of magnetic nanoparticles in the rapid monitoring of ochratoxin A. Orient. J. Chem. 33, 346–354. https://doi.org/10.13005/ojc/330141.

Sargazi, A., Azhoogh, M., Allahdad, S., Heidari Majd, M., 2018. Evaluation of supramolecule conjugated magnetic nanoparticles as a simultaneous carrier for methotrexate and tamoxifen. J. Drug Delivery Sci. Technol. 47, 115–122. https://doi.org/10.1016/j.jddst.2018.07.006.

Shahraki, S., Shiri, F., Heidari Majd, M., Dahmardeh, S., 2019. Anti-cancer study and whey protein complexation of new lanthanum (III) complex with the aim of achieving bioactive anticancer metal-based drugs. J. Biomol. Struct. Dyn. 37, 2072–2085. https://doi.org/10.1080/07391102.2018.1476266.

Shahraki, S., Shiri, F., Razmara, Z., Majd, M.H., 2019. A comparative study of the impact of metal complex size on the in vitro biological behavior of hetero di- and poly-nuclear Mn-Co complexes. J. Mol. Struct. 1178, 617–629. https://doi.org/10.1016/j.molstruc.2018.10.074.

Shen, S., Wu, Y., Liu, Y., Wu, D., 2017. High drug-loading nanomedicines: progress, current status, and prospects. Int. J. Nanomed. 12, 4085–4109. https://doi.org/10.2147/IJN.S132780.

Singh, D., McMillan, J.M., Liu, X.M., et al, 2014. Formulation design facilitates magnetic nanoparticle delivery to diseased cells and tissues. Nanomedicine (London, England) 9, 469–485. https://doi.org/10.2217/nnm.14.4.

Sorinezami, Z., Mansouri-Torshizi, H., Aminzadeh, M., et al, 2019. Synthesis of new ultrasonic-assisted palladium oxide nanoparticles: an in vitro evaluation on cytotoxicity and DNA/BSA binding properties. J. Biomol. Struct. Dyn. 37, 4238–4250. https://doi.org/10.1080/07391102.2018.1546619.

Stepan, T., Tété, L., Laundry-Mottiar, L., et al, 2022. Effect of nanoparticle size on the near-surface pH-distribution in aqueous and carbonate buffered solutions. Electrochim. Acta 409,. https://doi.org/10.1016/j.electacta.2022.139923 139923.

Subhan, M.A., Yalamarty, S.S.K., Filipczak, N., et al, 2021. Recent Advances in Tumor Targeting via EPR Effect for Cancer Treatment. J. Pers. Med. 11, 571. https://doi.org/10.3390/jpm11060571.

Theodosis-Nobelos, P., Charalambous, D., Triantis, C., Rikkou-Kalourkoti, M., 2020. Drug Conjugates Using Different Dynamic Covalent Bonds and their Application in Cancer Therapy. Curr. Drug Deliv. 17, 542–557. https://doi.org/10.2174/1567201817999200508092141.

Tilaki, R.M., 2007. A.I.S.The effect of liquid environment on size and aggregation of gold nanoparticles prepared by pulsed laser ablation. J. Nanopart. Res. 9, 853–860. https://doi.org/10.1007/s11051-006-9143-0.

Tzifi, F., Economopoulou, C., Gourgiotis, D., et al, 2012. The Role of BCL2 Family of Apoptosis Regulator Proteins in Acute and Chronic Leukemias. Adv Hematol 2012, 524308. https://doi.org/10.1155/2012/524308.

Wong, R.S.Y., 2011. Apoptosis in cancer: from pathogenesis to treatment. J Exp. Clin. Cancer Res. 30, 87. https://doi.org/10.1186/1756-9966-30-87.

Yan, Y., Dong, Y., Yue, S., et al, 2019. Dually Active Targeting Nanomedicines Based on a Direct Conjugate of Two Purely Natural Ligands for Potent Chemotherapy of Ovarian Tumors. ACS Appl. Mater. Interfaces 11, 46548–46557. https://doi.org/10.1021/acsami.9b17223.

Yang, L., Heidari Majd, M., Shiri, F., et al, 2021. The in vitro apoptotic effect of new zinc complex possessing folic acid and phenanthroline on cervix cancer cells. Appl. Organomet. Chem. https://doi.org/10.1002/aoc.6525.

Yoshida, N., Ikemoto, S., Narita, K., et al, 2002. Interleukin-6, tumour necrosis factor alpha and interleukin-1beta in patients with renal cell carcinoma. Br. J. Cancer 86, 1396–1400. https://doi.org/10.1038/sj.bjc.6600257.

Yu, C., Heidari Majd, M., Shiri, F., et al, 2021. The role of folic acid in inducing of apoptosis by zinc(II) complex in ovary and cervix cancer cells. Mol. Diversity. https://doi.org/10.1007/s11030-021-10293-5.

Yu, M., Xue, Y., Ma, P.X., et al, 2017. Intrinsic Ultrahigh Drug/miRNA Loading Capacity of Biodegradable Bioactive Glass Nanoparticles toward Highly Efficient Pharmaceutical Delivery. ACS Appl. Mater. Interfaces 9, 8460–8470. https://doi.org/10.1021/acsami.6b13874.

Zhang, R., Xing, R., Jiao, T., et al, 2016. Carrier-Free, Chemophotodynamic Dual Nanodrugs via Self-Assembly for Synergistic Antitumor Therapy. ACS Appl. Mater. Interfaces 8, 13262–13269. https://doi.org/10.1021/acsami.6b02416.

Zhang, R., Jiang, Y., Hao, L., et al, 2022. CD44/Folate Dual Targeting Receptor Reductive Response PLGA-Based Micelles for Cancer Therapy. Front Pharmacol 13,. https://doi.org/10.3389/fphar.2022.829590 829590.

Zhang, X., Lin, Y., Gillies, R.J., 2010. Tumor pH and Its Measurement. J. Nucl. Med. 51, 1167–1170. https://doi.org/10.2967/jnumed.109.068981.